Technical Note

Measurement of Brain Iron Distribution in Hallevorden-Spatz Syndrome

Jerzy Szumowski, PhD,[1*] Erhan Bas, MD,[2] Kirsten Gaarder, MD,[3] Erwin Schwarz,[1] Deniz Erdogmus, PhD,[2] and Susan Hayflick, MD[4]

Purpose: To investigate spatial distribution of iron accumulation in the globus pallidus (GP) in patients with Hallevorden-Spatz syndrome (HSS) using phase imaging. We compared sensitivity of a phase imaging technique to relaxation rate measurement methods (R1,R2,R2*) for iron quantification.

Materials and Methods: R1, R2, and R2* were measured in GP structure of the brain of eight pantothenate kinase-associated neurodegeneration (PKAN) patients and a healthy volunteer using a 3T magnetic resonance imaging (MRI) scanner. The phase of gradient-echo images was preprocessed to eliminate phase 2π wrapping and filtered to remove phase background variations. Phase gap across GP structure was used as a metric for iron effects quantification.

Results: Among the relaxation rates the most sensitive to iron accumulation was the R2* rate. The R1 and R2 rates demonstrated only small variations in this group of subjects. Up to an order of magnitude phase gap changes were measured between one PKAN patient and an age-matched healthy volunteer. Assuming that phase gap differences scale linearly with iron concentration we estimate that up to 2 mg Fe/g ww accumulates in GP of these patients.

Conclusion: Our results demonstrate significantly higher sensitivity of the phase measurements for quantitative assessment of iron concentration compared to the relaxation rate measurements. Phase measurements could potentially be used for monitoring a progression and a response to therapy in PKAN.

DEPOSITION OF IRON in the brain is thought to play a role in the pathophysiology of the normal aging process and neurodegenerative diseases (1–6). Whereas iron is required for normal neuronal metabolism, excessive levels can contribute to the formation of free radicals, leading to lipid peroxidation and neurotoxicity (4,7). Hallevorden-Spatz syndrome (HSS), also known as pantothenate kinase-associated neurodegeneration (PKAN), is an autosomal recessive disorder characterized by basal ganglia degeneration with excessive iron accumulation and pigmentary retinopathy. The disorder is caused by mutations in PANK2, one of four human pantothenate kinase genes to encode this key regulatory enzyme in the biosynthesis of coenzyme A (CoA) (8). The link between deficiency of pantothenate kinase 2 and the cardinal feature, excessive iron deposition in the basal ganglia, remains unclear. There is, however, a correlation between brain iron deposition and disease severity (9). Thus, a better understanding of the iron accumulation and spatial distribution in PKAN will improve monitoring of disease progression and may generate new ideas for therapeutics.

Magnetic resonance imaging (MRI) is a noninvasive technique with the potential to provide qualitative and quantitative assessment of iron distribution and concentration in vivo (3,5,7,10). The standard MRI studies of PKAN patients have usually demonstrated bilateral central areas of hyperintensity within a region of surrounding hypointensity in the medial globus pallidus (GP) on T2-weighted (T2w) and T2*-weighted (T2*w) images, a pattern known as the "eye-of-the-tiger" (EoT) sign (9,11). The area of hypointensity histologically corresponds to a zone of pathologically increased iron deposits, whereas the area of high signal intensity reflects loose tissue and gliosis (12) (Fig. 1).

Iron deposition changes both signal magnitude and phase of brain MR images (13). The methods for iron

Figure 1. The standard MRI studies of PKAN patients have usually demonstrated bilateral central areas of hyperintensity within a region of surrounding hypointensity in the medial globus pallidus (GP) on T2-weighted images (T2w), a pattern known as the "eye-of-the-tiger" (EoT) sign **(A)**. T1-weighted images (T1w) usually demonstrates a slight hyperintensity in the GP **(B)**.
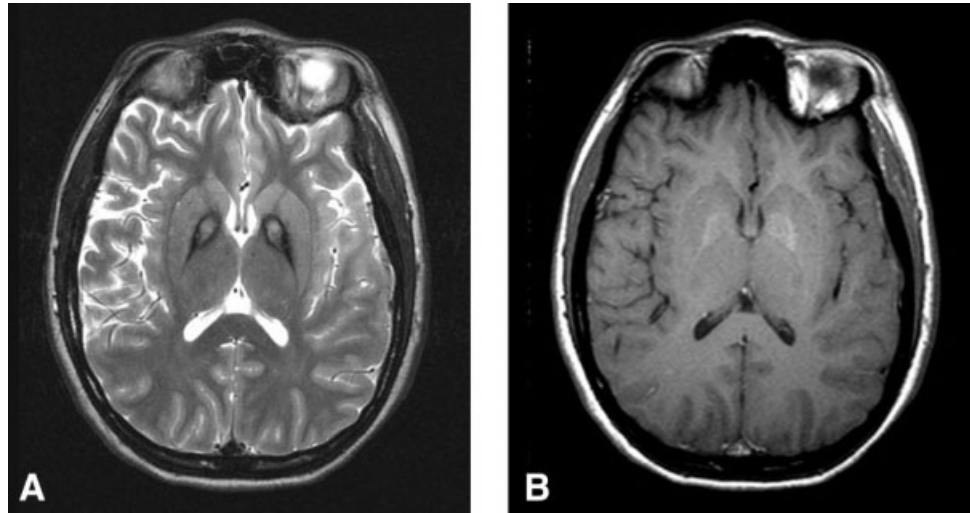
quantification based on signal magnitude changes have been developed and include measurements of T1, T2, T2', and T2* relaxation times (7,14–16). It has been shown that these quantitative MRI techniques based on magnitude changes of the MRI signal partially correlate with iron content within a limited range of iron concentration, as seen in an aging brain (17,18). The qualitatively observable increases of iron deposition have been described in various chronic neurological diseases such as in multiple sclerosis, Alzheimer's disease, Parkinson's disease, and PKAN; however, no quantitative iron concentration estimates have been reported based on MRI signal magnitude measurements (1,15,19–21). Moreover, at present there appears to be lack of consensus on the most desirable MRI method based on signal magnitude for accurately estimating iron content in the brain (2).

The phase of MRI can be an excellent source of contrast (13). In a review article by Haacke et al the authors state that the phase of the MRI signal could be the most accurate MRI means to map iron content, while T1 and T2 relaxation times would play important yet complementary roles (22,23). This has already been demonstrated for gray matter / white matter contrast, small veins in the brain, and more recently in venous blood vessels in the peripheral vasculature (22,24). A new approach in MRI referred to as susceptibility-weighted imaging (SWI) offers a means to quantify iron content differences between tissues in the brain based on local phase differences to map the iron (24–26).

Despite great promise, the effects of iron accumulation on the phase of MRI have only begun to be explored. The main reason for slow adoption of phase-based methods is the computation required to properly extract phase data from the source gradient-echo images. Analysis of MR image phase variations may be confounded by numerous background factors such as global magnetic field inhomogeneities, nonuniform radiofrequency (RF) penetration, magnetic field gradients from air–tissue interfaces, eddy currents, etc. These artifacts lead to phase rolling and phase 2π wrapping and must be eliminated or at least mini-

mized before true iron-related effects on phase can be assessed (27).

The aim of this study was to investigate the pattern of pathological iron accumulation within the globus pallidus structure in a group of eight patients with PKAN and a healthy volunteer using phase imaging. To assess the relative potential of magnitude methods to measure excessive iron concentration in PKAN disease we also performed quantitative measurements of T1, T2, and T2* relaxation times in this group of subjects.

We used phase gap changes across globus pallidus as a metric for iron concentration assessment (23). We demonstrate that the phase metrics exhibit a multifold increase in phase variations while magnitude methods demonstrated much smaller differentiation between healthy volunteers and PKAN patients.

MATERIALS AND METHODS

This study was reviewed and approved by the Oregon Health & Science University Investigational Review Board and all subjects signed an Informed Consent Form.

Relaxation Time T1, T2, and T2* Measurements

Brain MR images were acquired on a 3T Philips MRI scanner using a transmit/receive head coil. Eight PKAN patients (five males and three females, ages 13 to 21, average 16) and one healthy volunteer (male, age 17) were imaged. Following localizer images, standard T1 and T2 scans in the axial plane with 256 × 192 resolution matrix, field of view (FOV) = 20 cm, and slice thickness 4 mm were collected. For phase imaging, gradient-echo images (GRE) with the same geometrical parameters and a flip angle of 60° were acquired. Example images are presented in Fig. 1 with the following sequence parameters: T1-weighted scan: spin-echo sequence (SE) with TR/TE 550/8 msec. T2-weighted scan: turbo spin-echo sequence (TSE) (TR/TE 6000/80 msec and echo train 11). T2*-
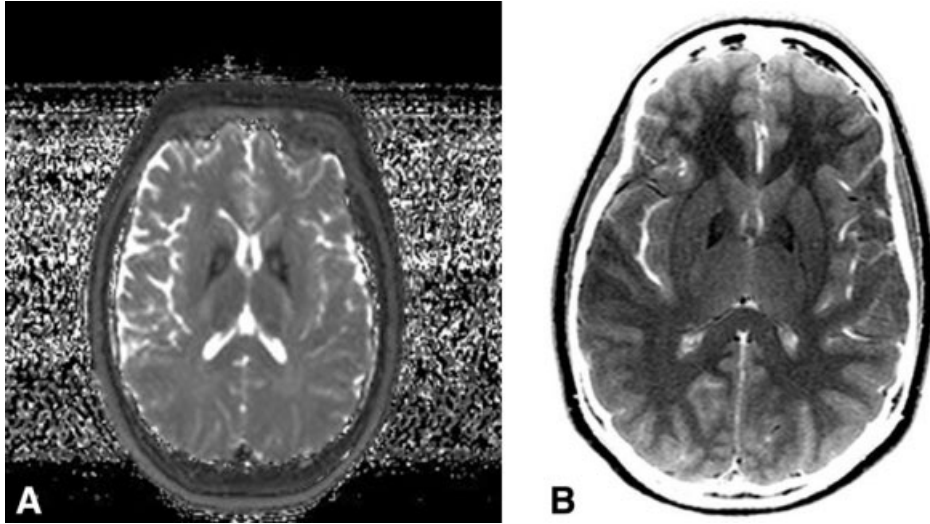
Figure 2. Reconstructed T2 map **(A)** and T1 map **(B)** images using a MIX sequence. These images were subsequently used to calculate T2 and T1 relaxation times in the GP region.

weighted scan: GRE with double-echo acquisition with TR = 1100 msec, TE1 = 5 msec, and TE2 = 25 msec. These images were saved in amplitude as well as phase format for T2* calculations and for image phase processing.

Relaxation parameters T1 and T2 were extracted from the MIX sequence consisting of a multiecho spin-echo sequence interleaved with a multiecho inversion-recovery sequence. The sequence has been described previously and is available as a product on a Philips platform (28).

For relaxation times analysis from the MIX sequence the GP was divided into two segments: an "eye" and a "rim." For calculation purposes the areas of interest were manually traced on images and the average relaxation time and standard deviation calculated over a selected segment. In addition to the GP, relaxation times were calculated in frontal lobe gray matter (GM) and in white matter (WM).

T2* times were calculated using a GRE double-echo gradient echo sequence with the first echo time TE1 = 5 msec and the second echo-time TE2 = 25 msec. The T2* values where calculated for each pixel using a known formula for signal S dependence on TE time in GRE sequence:

$$S\,(TE) = S0 \exp\,(-TE/T2*) \qquad [1]$$

From Eq. [1] the T2* relaxation time was calculated:

$$T2* = (TE2 - TE1)/\ln\,[S\,(TE1)/S\,(TE2)] \qquad [2]$$

The average relaxation time T2* and standard deviation were calculated over the selected regions.

Phase Measurements

Our phase processing involved a two-step process. First, gradient-echo phase data was preprocessed using a region-growing phase unwrapping algorithm (29,30). This step removed 2π phase wrapping in images. In the second step the remaining variations of the phase across an image were removed using a Hann filter.

For the removal of the background phase variations other groups have employed a highpass filter applied to raw image data (24,25). This approach used in susceptibility imaging enhances visualization of veins in the brain. The small veins are 1 mm or a fraction of a mm in diameter and the highpass filtering works reasonably well to eliminate phase variations without
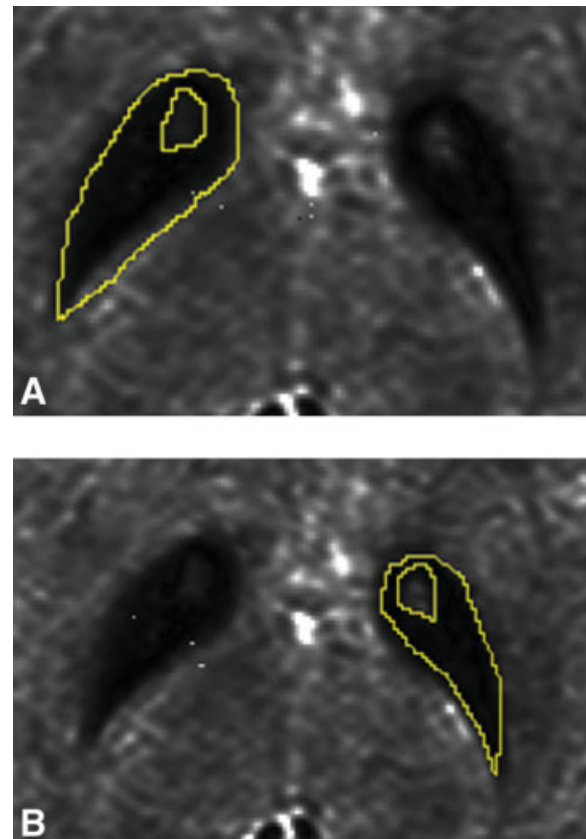
Figure 3. Segmentation of the "Eye" of the eye-of-tiger and the "Rim" in the left and right globus pallidus **(A,B)**. Relaxation parameters T1, T2, T2* were calculated on a per-pixel basis and and the average relaxation time and standard deviation calculated over a selected segment. Data are summarized in Table 1.

Table 1
T1, T2, and T2* Relaxation Time Measurements in GP

Subject	Eye			Rim		
	T1	T2	T2*	T1	T2	T2*
1	955 (45)	90 (12)	30 (6)	505 (62)	40 (13)	10 (4)
2	910 (52)	75 (14)	12 (7)	610 (75)	50 (17)	12 (6)
3	870 (44)	80 (10)	No data	710 (69)	40 (15)	No data
4	1005 (72)	70 (11)	22 (5)	655 (70)	50 (15)	8 (4)
5	1060 (59)	112 (19)	38 (8)	620 (70)	55 (19)	10 (6)
6	870 (47)	118 (12)	41 (12)	595 (66)	62 (21)	11 (4)
7	925 (63)	89 (16)	24 (8)	540 (63)	46 (17)	9 (5)
8	950 (59)	125 (11)	28 (8)	800 (92)	60 (25)	12 (5)
Healthy volunteer	825 (41)	101 (16)	32 (8)	825 (88)	101 (17)	32 (4)

Times are in msec units with standard deviation in parentheses.

undesirably altering the signal from the veins themselves. Unfortunately, the highpass filter is not an optimal filtering method for larger structures such as GP as its application significantly alters the native phase evolution across the GP structure. These issues have recently been revisited and a novel processing algorithm proposed (31).

In the second step of phase filtering we used a Hann window filter applied to the already unwrapped phase datasets. We experimented with various sizes of a window that included 16, 32, and 64 pixel size windows. We found out that a window of a size of 32 pixels provided the most reliable phase smoothing for all the subjects studied in this work.

Phase data processing was implemented in the MatLab (32) programming environment. 2D GRE images axial images containing the GP structure were acquired in six PKAN patients and one healthy volunteer. In addition, in two more PKAN patients (siblings) the phase data were collected in a coronal plane containing the GP structure. All brain image datasets acquired in this study have been processed using the two-step process described above.

RESULTS
Relaxation Time Measurements

Examples of reconstructed T2 and T1 relaxation time maps from the MIX sequence image dataset are shown in Fig. 2 and an example of GP segmentation is shown in Fig. 3.

Averaged relaxation time T1, T2, and T2* measurements in GP of an "eye" and a "rim" segments and in GM and WM are summarized in Table 1. The relaxa-

tion times were further converted to relaxation rates R1, R2, and R2* (as reciprocals of corresponding relaxation times) for comparison with phase gap measurements Table 2.

Phase Measurements

An example of phase 2π unwrapping and background phase flattening using a 32-pixel size Hann window applied to GRE echo phase image (TE = 5 msec) is presented in Fig. 4.

A typical phase profile across GP after phase processing pointing to a dipole source of phase variation is shown in Fig. 5. We used phase gap measurements corresponding to a minimum and maximum phase (defined as a phase gap) as a metrics that, we believe, reflects the level of iron concentration in GP (23,33). The results of these measurements averaged for left and right GP in PKAN patients and results of phase profile measurements in a healthy volunteer are summarized in Table 3. In addition, we converted phase change measured in radians into a corresponding change of magnetic field deviation expressed in hertz.

As can be seen from the results in the Table 1, R1 and R2 rates demonstrated only small variations in this group of subjects. A higher sensitivity to iron accumulation exhibit (not surprisingly) R2* parameter, albeit, significantly less than phase gap measurements. A ratio of R2* and a ratio of phase gaps between the patients and a healthy volunteer were on average 3.2:1 and 5.3:1, respectively (Table 2). In addition, a striking, order of magnitude phase gap changes were measured between one PKAN patient

Table 2
PKAN Patients Averaged R2 and R2* Relaxation Rates and Averaged Phase Gap Changes Across GP and Corresponding Data for a Healthy Volunteer

	R2 [s^{-1}]		R2* [s^{-1}]		Phase gap [radians]
	"eye"	"rim"	"eye"	"rim"	GP
PKAN	11.2 (1)	20.3 (2)	41.5 (9)	99.05 (21)	1.3 (0.2)
Volunteer	9.9 (1)		31.3 (6)		0.24 (0.1)
Ratios	3.2				5.3

A ratio of R2* in the rim and a ratio of phase gaps between the patients and a healthy volunteer were on average 3.2:1 and 5.3:1, respectively.
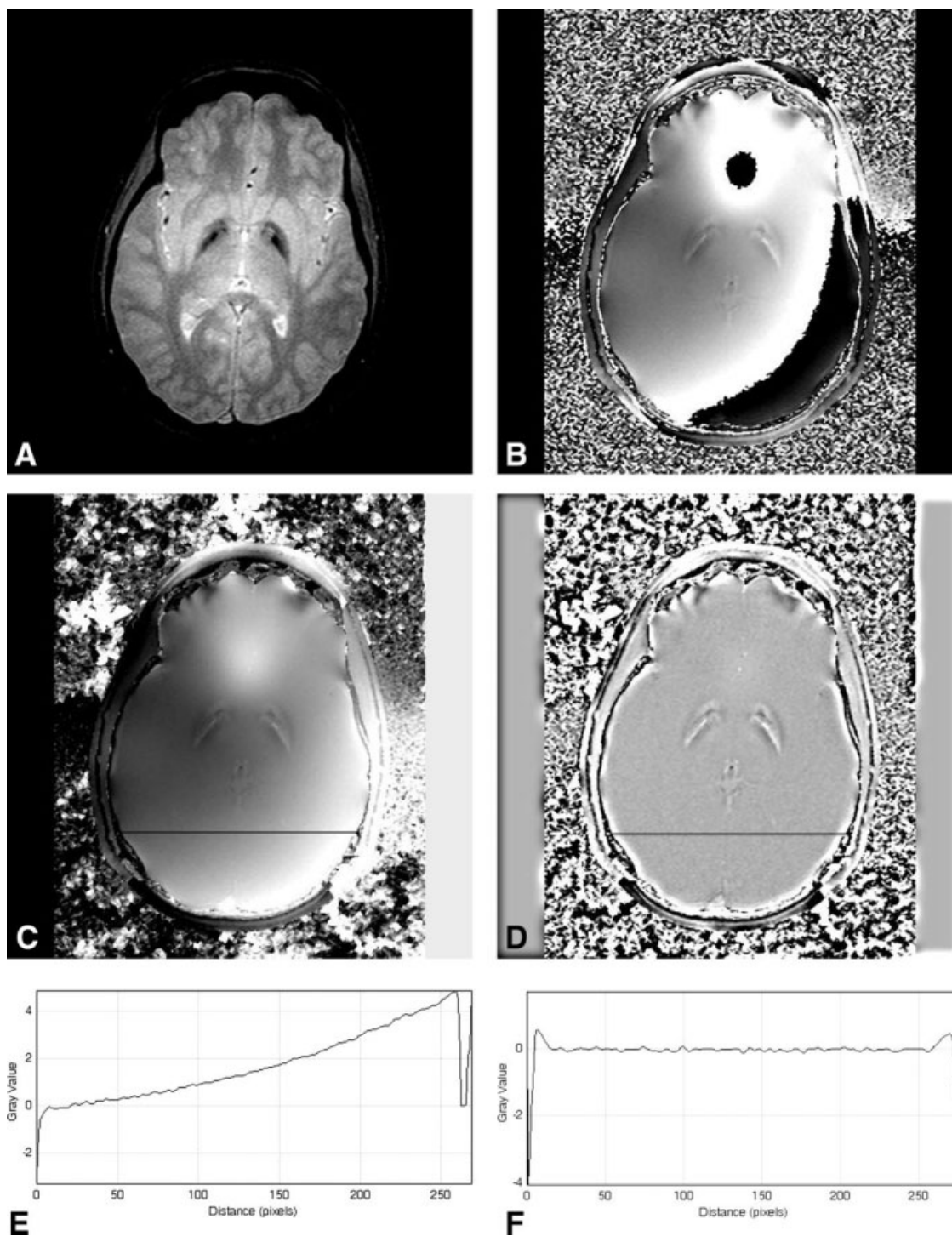
Figure 4. Processing of GRE image phase. Original GRE magnitude image **(A)** and corresponding phase image **(B)** acquired in an axial plane that contains GP. Phase image after phase unwrapping **(C)** and phase background filtering **(D)**. Phase profiles **(E)** and **(F)** are plotted for a line marked in (C) and (D), respectively. Note slow phase variations in (C,E) as compared to a smooth phase background in (D,F).

and an age-matched healthy volunteer (Table 3; data in bold).

DISCUSSION

Observable increases of iron deposition have been qualitatively described in various chronic neurological diseases such as in multiple sclerosis, Alzheimer's disease, Parkinson's disease, and PKAN. However, no specific quantitative iron concentration estimates have been reported (1,15,19,20). Quantitative methods that have been promoted as measures of iron accumulation in the brain are based on relaxation times T1, T2, T2*, and T2' or equivalent relaxation
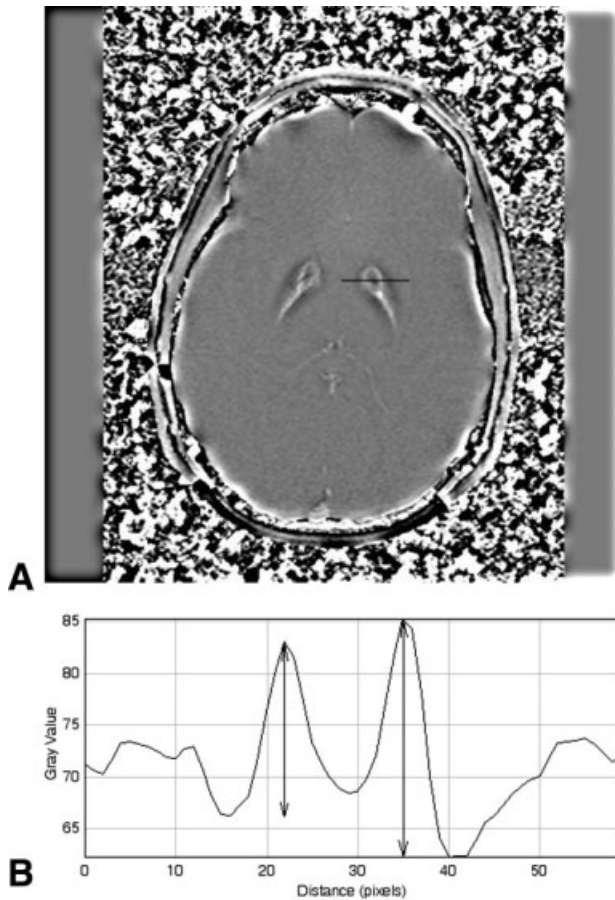
Figure 5. A typical processed phase (unwrapped and filtered) of a GRE image **(A)** and a profile of phase changes (in radians) across a GP region (black line in A) are shown in **B**. Measured phase gaps are indicated by arrows in (B).

rates R1, R2, R2*, and R2' measurements. It has been shown that these, to a certain degree, are correlated with tissue iron content in the elderly human subjects and in animal models (34). Recent results in nine normal subjects demonstrate a linear relationship between R2* measures and literature-derived iron concentration in four iron-rich areas of the brain: putamen, caudate nucleus, globus pallidus, and thalamus (35).

However, relaxation rates have not been shown to have the same predictive value in diseases that are known to be associated with iron accumulation. Moreover, at present there appears to be a lack of consensus on the most desirable MRI method based on signal magnitude for accurately estimating iron content in the diseased brain (2). This is further supported by this study, which found relatively minor differentiation between the subjects' T1 and T2 relaxation times.

We have shown that R2* relaxation rates, especially in the rim of GP, have a better potential to become surrogate indices for iron measures in PKAN patients. However, a new theory is needed to correlate actual R2* values with phase changes and iron concentration. Currently accepted theory stipulates that the spatial gradient of a local phase variation should correlate with R2* values (36). The spatial variation of the phase across GP in PKAN patients exhibits a typical dipolar pattern that can be appreciated in Fig. 6. The current theory is clearly not valid in cases of excessive accumulation of paramagnetic iron in a relatively small structure of the GP, which leads to a dipolar pattern of phase distribution. In addition, such a high concentration of iron makes T1 and T2 relaxations times together with a low spatial resolution H1 spectroscopy of limited use.

The most recent article describing relaxation and susceptibility characteristics in Hallevorde-Spatz syndrome provided only qualitative assessment of GP MRI features related to excessive iron accumulation (37). No attempt has been made to actually quantify iron stores. However, the ability to transition from a qualitative description of radiological features characteristic of PKAN disease to quantitative assessment of iron distribution and concentration would be extremely helpful in characterizing progression of this rare disease. Moreover, better relative quantification of brain iron could provide an outcome measure for clinical studies to evaluate experimental therapeutics in PKAN.

This is, to the best of our knowledge, the first study that utilizes image phase information to demonstrate its dipolar spatial character and uses phase changes across GP in an attempt to quantify iron stores in vivo in PKAN patients. The effect of iron on the phase of MRI is complex and leads to phase 2π wrapping;

Table 3
Results of Phase Difference (Gap) Measurements and Corresponding Magnetic Field Deviation

Subject	Phase difference		Magnetic field deviation	
	[radians]	SD [radians]	[Hz]	SD [Hz]
1	0.91	0.17	29.0	5.4
2	1.71	0.35	54.4	11.1
3	**2.32**	0.51	**73.8**	16.2
4	1.42	0.31	45.2	9.9
5	1.06	0.25	33.7	8.0
6	0.81	0.19	25.8	6.0
7	0.85	0.15	27.1	4.8
8	0.92	0.21	29.3	6.7
Healthy volunteer	**0.24**	0.04	**7.6**	1.3

Note that in one PKAN patient the phase gap difference is nearly an order of magnitude larger than phase change in a healthy volunteer (data in bold).
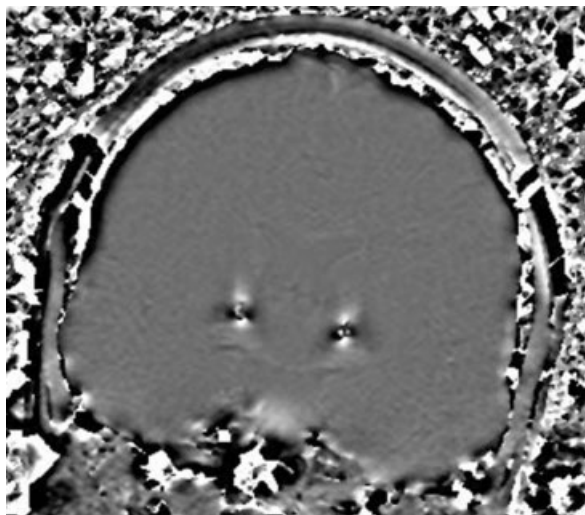
Figure 6. Results of phase processing for Subject 3. Note striking dipole pattern of phase distribution reflecting a strong iron accumulation of iron in GP of this patient.

thus, the phase must be unwrapped before iron distribution can be assessed. Furthermore, background phase variations must be removed before quantitative assessment of phase spatial distribution can be performed. In this work we developed a two-step phase processing approach to analyze image phase data that were collected using gradient-echo GRE technique on a high field strength 3T MRI scanner. It should be noted, however, that while image phase processing is necessary to unravel a true phase distribution over GP structure, such processing may lead to phase alteration, which could possibly affect the fidelity of phase profile data used in this study. More research is needed to develop robust phase processing algorithms that would remove background phase changes with a minimal distortion of a local phase. The metrics for the gap in phase across the GP have demonstrated better potential to characterize spatial distribution and quantitative iron accumulation then any of the magnitude-based methods. A ratio of R2* between the patients and a healthy volunteer and ratio of phase gaps were on average 3.2:1 and 5.3:1, respectively (Table 2). Moreover, up to an order of magnitude phase gap change was measured between one PKAN patient and an age-matched healthy volunteer (see Table 3). Assuming that phase gap differences scale linearly with iron concentration (33) and taking into account published data for iron concentration in the GP of healthy volunteers (3), we estimate that up to 2 mg Fe/g ww accumulates in the GP of these patients.

Our pilot study has certain limitations, and to prove that phase could indeed be a useful index of PKAN progression a number of necessary developmental steps are needed. Our current phase data are based on a planar 2D GRE acquisition with a limited spatial resolution. The slice thickness was 4 mm, which could potentially affect the phase analysis. We plan to continue this research with data acquisition using 3D GRE sequence with an isotropic image voxel. T2*

measurements could be improved as well by acquiring a train of multiple-echo gradient-echo images with very short echo times.

Our quantitative estimate of iron concentration in GP of PKAN patients is based on a comparison of phase changes across GP in a healthy volunteer. For more accurate iron concentration quantification a theoretical model would have to be developed that correlates the geometry of the GP structure, distribution of iron among the "eye" and the "rim," and phase variations across GP. Such models have been analytically described for simple spherical or cylindrical geometries of paramagnetic objects in a diamagnetic medium. More theoretical work would need to be done for the complex geometry of the GP before an accurate quantification of iron spatial distribution and focal concentration could be made. Work describing a method that uses a first-order perturbation approach to Maxwell's magnetostatic equations, combined with the Fourier transformation technique for calculating magnetic field in the presence of an arbitrary distribution of bulk susceptibility, offers promise that such a complex task could indeed be accomplished (38).

In conclusion, we believe that the strong differentiation of phase metrics between PKAN patients and a healthy subject indicates that phase could serve as a useful index of PKAN disease progression. Further work holds promise for developing a robust quantitative assessment of iron accumulation in this rare disease. This, in turn, will improve our understanding of how iron contributes to the disease process and may lead to the development of new avenues of therapy. Even more important, this potential outcomes measure, if validated, will finally open the door to experimental drug testing in PKAN. The ability to quantify and assess longitudinal changes in regional brain iron could improve our understanding of the complexity of the disease process. This would help to explicate pathogenesis, track disease progression, and monitor treatment effects.

REFERENCES

1. Bartzokis G, Cummings J, Perlman S, Hance DB, Mintz J. Increased basal ganglia iron levels in Huntington disease. Arch Neurol 1999;56:569–574.
2. Brass SD, Chen NK, Mulkern RV, Bakshi R. Magnetic resonance imaging of iron deposition in neurological disorders. Top Magn Reson Imaging 2006;17:31–40.
3. Haacke EM, Cheng NY, House MJ, et al. Imaging iron stores in the brain using magnetic resonance imaging. Magn Reson Imaging 2005;23:1–25.
4. Loeffler DA, Conner JR, Juneau PL, et al. Transferrin and iron in normal, Alzheimer's disease, and Parkinson's disease brain regions. J Neurochem 1995;65:710–716.
5. Schenck JF, Zimmerman EA. High-field magnetic resonance imaging of brain iron: birth of a biomarker? NMR Biomed 2004;17:433–445.
6. Vymazal J, Brooks RA, Patronas N, Hajek M, Bulte JW, Di Chiro G. Magnetic resonance imaging of brain iron in health and disease. J Neurol Sci 1995;134(Suppl):19–26.
7. Vymazal J, Hajek M, Patronas N, et al. The quantitative relation between T1-weighted and T2-weighted MRI of normal gray matter and iron concentration. J Magn Reson Imaging 1995;5:554–560.
8. Zhou B, Westaway SK, Levinson B, Johnson MA, Gitschier J, Hayflick SJ. A novel pantothenate kinase gene (PANK2) is

defective in Hallervorden-Spatz syndrome. Nat Genet 2001;28: 345–349.

9. Hayflick SJ, Westaway SK, Levinson B, et al. Genetic, clinical, and radiographic delineation of Hallervorden-Spatz syndrome. N Engl J Med 2003;348:33–40.

10. McNeill A, Birchall D, Hayflick SJ, et al. T2* and FSE MRI distinguishes four subtypes of neurodegeneration with brain iron accumulation. Neurology 2008;70:1614–1619.

11. Guillerman RP. The eye-of-the-tiger sign. Radiology 2000;217: 895–896.

12. Koyama M, Yagishita A. Pantothenate kinase-associated neurodegeneration with increased lentiform nuclei cerebral blood flow. AJNR Am J Neuroradiol 2006;27:212–213.

13. Haacke EM, Brown RW, Thompson MR, Venkatesan R. Magnetic resonance imaging. Physical principles and sequence design. New York: Wiley-Liss; 1999.

14. Brooks RA, Vymazal J, Goldfarb RB, Bulte JWM, Aisen P. Relaxometry and megnetometry of ferritin. Magn Reson Med 1998;40: 227–235.

15. Vymazal J, Righini A, Brooks RA, et al. T1 and T2 in the brain of healthy subjects, patients with Parkinson disease, and patients with multiple system atrophy: relation to iron content. Radiology 1999;211:489–495.

16. Ordidge RJ, Gorell JM, Deniau JC, Knight RA, Helpern JA. Assessment of relative brain iron concentrations using T2-weighted and T2*-weighted MRI at 3 Tesla. Magn Reson Med 1994;32:335–341.

17. Thomas LO, Boyko OB, Anthony DC, Burger PC. MR detection of brain iron. Am J Neuroradiol 1993;14:1043–1048.

18. Adams JH, Doyle D, Ford I, Gennarelli TA, Graham DI, McLellan DR. Diffuse axonal injury in head injury: definition, diagnosis and grading. Histopathology 1989;15:49–59.

19. Bartzokis G, Cummings JL, Markham CH, et al. MRI evaluation of brain iron in earlier- and later-onset Parkinson's disease and normal subjects. Magn Reson Imaging 1999;17:213–222.

20. Bartzokis G, Tishler TA. MRI evaluation of basal ganglia ferritin iron and neurotoxicity in Alzheimer's and Huntingon's disease. Cell Mol Biol (Noisy-le-grand) 2000;46:821–833.

21. Gorell JM, Ordidge RJ, Brown GG, Deniau JC, Buderer NM, Helpern JA. Increased iron-related MRI contrast in the substantia nigra in Parkinson's disease. Neurology 1995;45:1138–1143.

22. Haacke EM, Xu Y, Cheng YC, Reichenbach JR. Susceptibility weighted imaging (SWI). Magn Reson Med 2004;52:612–618.

23. Ogg RJ, Langston JW, Haacke EM, Steen RG, Taylor JS. The correlation between phase shifts in gradient-echo MR images and regional brain iron concentration. Magn Reson Imaging 1999;17: 1141–1148.

24. Reichenbach JR, Haacke EM. High-resolution BOLD venographic imaging: a window into brain function. NMR Biomed 2001;14: 453–467.

25. Haacke EM. Susceptibility weighted imaging (SWI). Z Med Phys 2006;16:237.

26. Wang Y, Yu Y, Li D, et al. Artery and vein separation using susceptibility-dependent phase in contrast-enhanced MRA. J Magn Reson Imaging 2000;12:661–670.

27. Duyn JH, van Gelderen P, Li TQ, de Zwart JA, Koretsky AP, Fukunaga M. High-field MRI of brain cortical substructure based on signal phase. Proc Natl Acad Sci U S A 2007;104: 11796–11801.

28. In den Kleef JJ, Cuppen JJ. RLSQ: T1, T2, and rho calculations, combining ratios and least squares. Magn Reson Med 1987;5: 513–524.

29. Ghiglia DC, Pritt MD. Two-dimensional phase unwrapping. Theory, algorithms and software. New York: John Wiley & Sons; 1998.

30. Szumowski J, Coshow W, Li F, Quinn SF. Phase unwrapping in 3-point Dixon method for fat suppression MRI. Radiology 1994; 192:555–561.

31. Rauscher A, Barth M, Herrman KH, Witoszyskij S, Deistung A, Reinchenbach JR. Improved elimination of phase effects from background field inhomogeneities for susceptibility weighted imaging at high magnetic field strengths. Magn Reson Imaging 2008;26:1135–1151.

32. MathWorks, Natick, MA.

33. Yamada N, Imakita S, Sakuma T, et al. Evaluation of the susceptibility effect on the phase images of a simple gradient echo. Radiology 1990;175:561–565.

34. Hardy PA, Gash D, Yokel R, Andersen A, Ai Y, Zhang Z. Correlation of R_2 with total iron concentration in the brains of rhesus monkeys. J Magn Reson Imaging 2005;21:118–127.

35. Yao B, Li TQ, Gelderen P, Shmueli K, de Zwart JA, Duyn JH. Susceptibility contrast in high field MRI of human brain as a function of tissue iron content. Neuroimage 2009;44:1259–1266.

36. Reichenbach JR, Venkatesan R, Yablonskiy DA, Thompson MR, Lai S, Haacke EM. Theory and application of static field inhomogeneity effects in gradient-echo imaging. J Magn Reson Imaging 1997;7:266–279.

37. Vinod Desai S, Bindu PS, Ravishankar S, Jayakumar PN, Pal PK. Relaxation and susceptibility MRI characteristics in Hallervorden-Spatz syndrome. J Magn Reson Imaging 2007;25:715–720.

38. Salmir R, Baudouin DDS, Moonen C. A fast calculation method for magnetic field inhomogeneity due to an arbitrary distribution of bulk susceptibility. Concepts Magn Reson B 2003: 126–134.